Considerations in the Calculation of Vertical Velocity in Three-Dimensional Circulation Models

RICHARD A. LUETTICH JR.

Institute of Marine Sciences, University of North Carolina at Chapel Hill, Morehead City, North Carolina

JULIA C. MUCCINO

Department of Civil and Environmental Engineering, Arizona State University, Tempe, Arizona

MICHAEL G. G. FOREMAN

Department of Fisheries and Oceans, Institute of Ocean Sciences, Sidney, British Columbia, Canada

(Manuscript received 9 January 2002, in final form 26 June 2002)

ABSTRACT

The vertical velocity, *w,* in three-dimensional circulation models is typically computed from the three-dimensional continuity equation given the free-surface elevation and depth-varying horizontal velocity. This problem appears to be overdetermined, since the continuity equation is first order, yet *w* must satisfy boundary conditions at both the free surface and the bottom. At least three methods have been previously proposed to compute *w*: (i) a ''traditional'' method that solves the continuity equation using only the bottom boundary condition, (ii) a ''vertical derivative'' method that solves the vertical derivative of the continuity equation using both boundary conditions, and (iii) an ''adjoint'' method that solves the continuity equation and both boundary conditions in a least squares sense. The latter solution is equivalent to the traditional solution plus a correction that varies linearly over the depth.

It is shown here that the vertical derivative method is mathematically and physically inconsistent if discretized as previously proposed. However, if properly discretized it is equivalent to the adjoint method if the boundary conditions are weighted so that they are satisfied exactly. Furthermore, if the surface elevation and horizontal velocity fields satisfy the depth-integrated continuity equation locally, one of the boundary conditions is redundant. In this case, the traditional, adjoint, and properly discretized vertical derivative approaches yield the same results for *w*. If the elevation and horizontal velocity are not locally mass conserving, the mass error is transferred into *w*. This is important for models that do not guarantee local mass conservation, such as some finite element models.

1. Introduction

This paper investigates the merits of different approaches for calculating vertical velocity fields by solving the three-dimensional continuity equation, assuming the free-surface elevation and horizontal velocity fields are known.

In typical three-dimensional circulation models, including the Dartmouth circulation models FUNDY (Lynch and Werner 1987) and QUODDY (Lynch and Werner 1991; Lynch and Naimie 1993), the Princeton Ocean Model (POM; Blumberg and Mellor 1987), and the Regional Ocean Model System (ROMS) (Haidvogel and Beckmann 1999), the vertical velocity is determined from the three-dimensional continuity equation:

$$\frac{\partial w}{\partial z} = -\nabla \cdot \mathbf{V}, \tag{1}$$

where $\mathbf{V}(x, y, z, t)$ is the horizontal velocity with components $[u(x, y, z, t), v(x, y, z, t)]$, and $w(x, y, z, t)$ is the vertical velocity. Here (x, y) are the horizontal coordinates, z is the vertical coordinate (positive upward, $z = 0$ at the mean water surface), t is time, and ∇ is the horizontal gradient operator. The kinematic boundary condition on vertical velocity at the bottom is

$$w = -\mathbf{V} \cdot \nabla h = w_b \quad \text{at } z = -h, \tag{2a}$$

where $h(x, y)$ is the mean water depth. The analogous condition at the surface is

$$w = \frac{\partial \eta}{\partial t} + \mathbf{V} \cdot \nabla \eta = w_s \quad \text{at } z = \eta, \tag{2b}$$

Corresponding author address: Dr. Julia C. Muccino, Dept. of Civil and Environmental Engineering, P.O. Box 875306, Arizona State University, Tempe, AZ 85287-5306.
E-mail: jcm@asu.edu

where $\eta(x, y, t)$ is the free-surface elevation. (Note, for future reference, that w_b has been defined as the vertical velocity at the bottom as determined from the boundary condition, and w_s has been defined as the vertical velocity at the surface as determined from the boundary condition.) Equations (1) and (2) are solved for w assuming that the horizontal velocity and surface elevations are known from a previous step in the model solution. The primary difficulty of solving these equations is that, together, they constitute an overdetermined system of equations for the most general case; that is, (1) is a *first*-order equation that must be solved subject to *two* boundary conditions. As will be shown, in numerical schemes that are locally mass conserving, one of the boundary conditions becomes redundant and, thus, the system is not overdetermined in that case.

We will consider here two approaches to solving the overdetermined system:

1) Solution of the vertical derivative of the continuity equation:

$$\frac{\partial^2 w_{\text{vdc}}}{\partial z^2} = -\frac{\partial}{\partial z}(\nabla \cdot \mathbf{V}), \tag{3}$$

   where w_{vdc} indicates vertical velocity computed using this approach (henceforth, VDC). This is a second-order differential equation, so both boundary conditions can be satisfied (Lynch and Naimie 1993).
2) Solution of the overdetermined system in a ''best fit'' sense by admitting residuals in the first-order continuity equation and both boundary conditions. An optimal solution is then sought that minimizes those residuals in a weighted least squares sense. Because this approach involves the adjoint of the continuity equation, we call it the ''adjoint'' approach (henceforth, ADJ). It will be described in more detail in section 3.

A third approach, called the ''traditional'' approach (TRAD) simply neglects one of the boundary conditions; this approach will be shown here to be a component of ADJ.

Muccino et al. (1997) found that VDC and ADJ provide different vertical velocity fields regardless of resolution in the vertical or horizontal and that ADJ better approximates the analytic solution in a simple test problem than does VDC. The objectives of this paper are to reconcile the numerical differences between VDC and ADJ and to make overall recommendations for the computation of vertical velocity in three-dimensional circulation models. Results are provided for tidally forced circulation in a quarter annular test case and a wind-, density-, and boundary-forced circulation off the southwest coast of Vancouver Island.

2. A summary of the adjoint approach

ADJ admits residuals in the continuity equation (1) and the boundary conditions (2) at each horizontal node:

$$f(z) = \frac{\partial w}{\partial z} + \nabla \cdot \mathbf{V}, \tag{4a}$$

$$i_b = w + \mathbf{V} \cdot \nabla h \qquad \text{at } z = -h, \tag{4b}$$

$$i_s = w - \frac{\partial \eta}{\partial t} - \mathbf{V} \cdot \nabla \eta \quad \text{at } z = \eta. \tag{4c}$$

A cost functional, which is formed from the squares of these residuals, is defined:

$$I = \frac{W_f}{H} \int_{-h}^{\eta} \{f\}^2 \, dz + W_b\{i_b\}^2 + W_s\{i_s\}^2, \tag{5}$$

where W_f, W_b, and W_s are constant weights, and $H(x, y, t) = h(x, y) + \eta(x, y, t)$ is the total water depth, included in the denominator of the first term to normalize the vertical integral and also to maintain dimensional consistency. The weights are defined as the inverses of the covariances of the residuals:

$$W_f = \frac{1}{C_f}, \qquad W_b = \frac{1}{C_b}, \qquad W_s = \frac{1}{C_s}, \tag{6}$$

where the covariances are defined as

$$C_f = \langle f^2 \rangle, \qquad C_b = \langle i_b^2 \rangle, \qquad C_s = \langle i_s^2 \rangle, \tag{7}$$

and $\langle\ \rangle$ indicates expected value. Thus, the dimensions of W_f, W_b, and W_s are T^2, T^2/L^2, and T^2/L^2, respectively. We will assume that $W_b = W_s$. Additionally, given that only the relative values of the weights are significant (not the absolute values of the weights themselves), we set $W_b = W_s = 1$ without further loss of generality. Thus, (5) can be written

$$I = \frac{W_f}{H} \int_{-h}^{\eta} f^2 \, dz + i_b^2 + i_s^2. \tag{8}$$

The adjoint solution, w_{adj}, minimizes I and can be shown to be

$$w_{\text{adj}}(z) = w_{\text{trad}}(z) + w_c(z),$$

$$w_c(z) = [w_s - w_{\text{trad}}(\eta)]\frac{W_f/H^2 + (h + z)/H}{2W_f/H^2 + 1}, \tag{9}$$

where w_{trad} is the ''traditional solution'' to the governing equation (1) and the bottom boundary condition (2a). [For mathematical details leading to (9) see Muccino et al. (1997); for a similar derivation using ''representers,'' see, e.g., Muccino and Bennett (2002), their appendix A] Thus, the adjoint solution is a sum of w_{trad} and a correction that is linear in z and proportional to the misfit between the traditional solution evaluated at the surface and the surface boundary condition. In the limit of $W_f/H^2 = 0$ (i.e., no weight given to the three-dimensional continuity equation in I), the correction reduces to

$$w_c(z) = [w_s - w_{\text{trad}}(\eta)]\frac{h + z}{H} \quad \text{for } \frac{W_f}{H^2} = 0. \tag{10}$$

In this case, the correction is zero at the bottom and

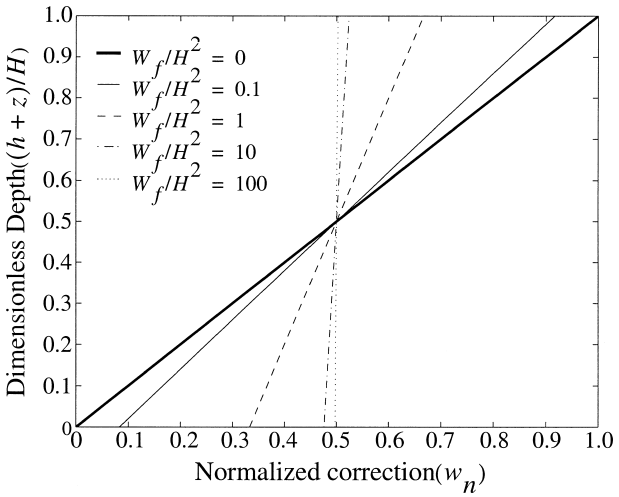

FIG. 1. Normalized ADJ correction profiles for a range of W_f/H^2. For $W_f/H^2 = 0$, the normalized correction ranges from 0.0 at the bottom to 1.0 at the top. For large W_f/H^2, the normalized misfit approaches a constant value of 0.5.

equal to the surface boundary condition misfit of the traditional solution at the surface. Consequently, the correction causes the adjoint solution to satisfy both boundary conditions exactly, although it may diminish the mass-conserving properties of the solution. In the limit of $W_f/H^2 \to \infty$ (i.e., no weight given to the boundary conditions in I), (9) reduces to

$$w_c(z) = \frac{w_s - w_{\text{trad}}(\eta)}{2} \quad \text{for } W_f \to \infty. \tag{11}$$

In this case, the correction approaches a constant (half of the misfit between the traditional solution evaluated at the surface and the surface boundary condition) over the depth. This distributes any error evenly between the surface and bottom boundary conditions but has no impact on the mass-conserving property of the solution. Clearly, intermediate values of W_f/H^2 generate corrections that fall between these limits. These observations are illustrated in Fig. 1, which shows the correction, normalized by the surface boundary condition misfit

$$w_n(z) = \frac{w_c(z)}{w_s - w_{\text{trad}}(\eta)} = \frac{W_f/H^2 + (h + z)/H}{2W_f/H^2 + 1} \tag{12}$$

for various values of W_f/H^2.

3. Numerical implementation

Two approaches to determining the vertical velocity have been described and will now be tested numerically. A vertical sequence of three nodes indicated by subscripts $i - 1$, i, and $i + 1$ will be used, as shown in Fig. 2. Superscripts $-$ and $+$ indicate quantities evaluated over the intervals $\{i - 1, i\}$ and $\{i, i + 1\}$, respectively (e.g., $\Delta z^+ = z^{i+1} - z_i$). In each case, we

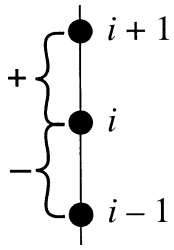

FIG. 2. Notation used for vertical discretization.

assume that the vertical velocity is computed at the same nodes as the horizontal velocity.

Most three-dimensional circulation models use stretched or terrain-following coordinates in which the vertical dimension is transformed from $-h < z < \eta$ to $b < \sigma < a$, where a and b are arbitrary constants (e.g., $a = 1$, $b = 0$):

$$\sigma = a + \frac{(a + b)(z - \eta)}{H}. \tag{13}$$

Derivatives in the terrain-following coordinate system are related to derivatives in the level coordinate system using the chain rule:

$$\nabla \cdot \mathbf{V} = \nabla_\sigma \cdot \mathbf{V} - \frac{(a - b)}{H}\left[\frac{(\sigma - b)}{(a - b)}\nabla\eta + \frac{(\sigma - a)}{(a - b)}\nabla h\right] \cdot \frac{\partial \mathbf{V}}{\partial \sigma}, \tag{14a}$$

$$\frac{\partial}{\partial z} = \frac{(a - b)}{H}\frac{\partial}{\partial \sigma}, \tag{14b}$$

where ∇ indicates horizontal derivatives on a level surface, and ∇_σ indicates horizontal derivatives on a stretched surface.

a. Discretization of VDC

Using centered finite difference, the lhs of (3) can be discretized:

$$\frac{\partial^2 w_{\text{vdc}}}{\partial z^2} = \frac{\partial}{\partial z}\left(\frac{\partial w_{\text{vdc}}}{\partial z}\right) \approx \frac{\left(\frac{\partial w_{\text{vdc}}}{\partial z}\right)^+ - \left(\frac{\partial w_{\text{vdc}}}{\partial z}\right)^-}{\frac{1}{2}(\Delta z^+ + \Delta z^-)}$$

$$= \frac{\left(\frac{w_{\text{vdc}}^{i+1} - w_{\text{vdc}}^i}{\Delta z^+}\right) - \left(\frac{w_{\text{vdc}}^i - w_{\text{vdc}}^{i-1}}{\Delta z^-}\right)}{\frac{1}{2}(\Delta z^+ + \Delta z^-)}$$

$$= \frac{2}{(\Delta z^+ + \Delta z^-)} \times \left[\frac{w_{\text{vdc}}^{i+1}}{\Delta z^+} - w_{\text{vdc}}^i\left(\frac{1}{\Delta z^+} + \frac{1}{\Delta z^-}\right) + \frac{w_{\text{vdc}}^{i-1}}{\Delta z^-}\right]; \quad (15)$$

and the rhs of (3) can be discretized:

$$-\frac{\partial}{\partial z}(\nabla \cdot \mathbf{V}) \approx -\frac{(\nabla \cdot \mathbf{V})^+ - (\nabla \cdot \mathbf{V})^-}{\frac{1}{2}(\Delta z^+ + \Delta z^-)} = -\frac{2}{(\Delta z^+ + \Delta z^-)}\frac{1}{2}\{[(\nabla \cdot \mathbf{V})^{i+1} + (\nabla \cdot \mathbf{V})^i] - [(\nabla \cdot \mathbf{V})^i + (\nabla \cdot \mathbf{V})^{i-1}]\}. \quad (16)$$

Combining (15) and (16) yields

$$\frac{w_{\text{vdc}}^{i+1}}{\Delta z^+} - w_{\text{vdc}}^i\left(\frac{1}{\Delta z^+} + \frac{1}{\Delta z^-}\right) + \frac{w_{\text{vdc}}^{i-1}}{\Delta z^-} = -\frac{1}{2}\{[(\nabla \cdot \mathbf{V})^{i+1} + (\nabla \cdot \mathbf{V})^i]^+ - [(\nabla \cdot \mathbf{V})^i + (\nabla \cdot \mathbf{V})^{i-1}]^-\}, \quad (17)$$

where the + and − have been added to the two terms inside the curly brackets of (17) as a reminder that the first group in square brackets is evaluated over the interval $\{i, i + 1\}$ and the second group is evaluated over the interval $\{i - 1, i\}$.

The lhs of (17) is tridiagonal and efficiently solved using a tridiagonal solver like the Thomas algorithm. The rhs of (17) requires the evaluation of the horizontal velocity derivatives on level coordinate surfaces. Using (14a) and (14b) to expand terms on the rhs of (17) gives, in terms of horizontal derivatives on stretched surfaces,

$$[(\nabla \cdot \mathbf{V})^{i+1}]^+ = (\nabla_\sigma \cdot \mathbf{V})^{i+1} - \frac{(a-b)}{H}\left[\left(\frac{\sigma^{i+1} - b}{a - b}\right)\nabla\eta + \left(\frac{\sigma^{i+1} - a}{a - b}\right)\nabla h\right] \cdot \left(\frac{\mathbf{V}^{i+1} - \mathbf{V}^i}{\Delta\sigma^+}\right), \quad (18a)$$

$$[(\nabla \cdot \mathbf{V})^i]^+ = (\nabla_\sigma \cdot \mathbf{V})^i - \frac{(a-b)}{H}\left[\left(\frac{\sigma^i - b}{a - b}\right)\nabla\eta + \left(\frac{\sigma^i - a}{a - b}\right)\nabla h\right] \cdot \left(\frac{\mathbf{V}^{i+1} - \mathbf{V}^i}{\Delta\sigma^+}\right), \quad (18b)$$

$$[(\nabla \cdot \mathbf{V})^i]^- = (\nabla_\sigma \cdot \mathbf{V})^i - \frac{(a-b)}{H}\left[\left(\frac{\sigma^i - b}{a - b}\right)\nabla\eta + \left(\frac{\sigma^i - a}{a - b}\right)\nabla h\right] \cdot \left(\frac{\mathbf{V}^i - \mathbf{V}^{i-1}}{\Delta\sigma^-}\right), \quad (18c)$$

$$[(\nabla \cdot \mathbf{V})^{i-1}]^- = (\nabla_\sigma \cdot \mathbf{V})^{i-1} - \frac{(a-b)}{H}\left[\left(\frac{\sigma^{i-1} - b}{a - b}\right)\nabla\eta + \left(\frac{\sigma^{i-1} - a}{a - b}\right)\nabla h\right] \cdot \left(\frac{\mathbf{V}^i - \mathbf{V}^{i-1}}{\Delta\sigma^-}\right). \quad (18d)$$

Substituting (18a)–(18d) into (17), and recognizing that $\Delta z = H\Delta\sigma/(a - b)$, yields

$$\frac{w_{\text{vdc}}^{i+1}}{\Delta\sigma^+} - w_{\text{vdc}}^i\left(\frac{1}{\Delta\sigma^+} + \frac{1}{\Delta\sigma^-}\right) + \frac{w_{\text{vdc}}^{i-1}}{\Delta\sigma^-} = -\frac{1}{2}\left\{\frac{H}{(a-b)}[(\nabla_\sigma \cdot \mathbf{V})^{i+1} + (\nabla_\sigma \cdot \mathbf{V})^i]^+ - \frac{H}{(a-b)}[(\nabla_\sigma \cdot \mathbf{V})^i + (\nabla_\sigma \cdot \mathbf{V})^{i-1}]^- - \left[\frac{(\sigma^{i+1} + \sigma^i - 2b)}{(a-b)}\nabla\eta + \frac{(\sigma^{i+1} + \sigma^i - 2a)}{(a-b)}\nabla h\right] \cdot \left(\frac{\mathbf{V}^{i+1} - \mathbf{V}^i}{\Delta\sigma^+}\right) + \left[\frac{(\sigma^i + \sigma^{i-1} - 2b)}{(a-b)}\nabla\eta + \frac{(\sigma^i + \sigma^{i-1} - 2a)}{(a-b)}\nabla h\right] \cdot \left(\frac{\mathbf{V}^i - \mathbf{V}^{i-1}}{\Delta\sigma^-}\right)\right\}. \quad (19)$$

In practice, the horizontal derivatives $[(\nabla_\sigma \cdot \mathbf{V})^i]^+ = [(\nabla_\sigma \cdot \mathbf{V})^i]^-$, and therefore (19) reduces to

$$\frac{w_{\text{vdc}}^{i+1}}{\Delta\sigma^+} - w_{\text{vdc}}^i\left(\frac{1}{\Delta\sigma^+} + \frac{1}{\Delta\sigma^-}\right) + \frac{w_{\text{vdc}}^{i-1}}{\Delta\sigma^-} = -\frac{1}{2}\left\{\frac{H}{(a-b)}[(\nabla_\sigma \cdot \mathbf{V})^{i+1} - (\nabla_\sigma \cdot \mathbf{V})^{i-1}] - \left[\frac{(\sigma^{i+1} + \sigma^i - 2b)}{(a-b)}\nabla\eta + \frac{(\sigma^{i+1} + \sigma^i - 2a)}{(a-b)}\nabla h\right] \cdot \left(\frac{\mathbf{V}^{i+1} - \mathbf{V}^i}{\Delta\sigma^+}\right)\right.$$

$$+\left[\frac{(\sigma^i+\sigma^{i-1}-2b)}{(a-b)}\nabla\eta + \frac{(\sigma^i+\sigma^{i-1}-2a)}{(a-b)}\nabla h\right]\cdot\left(\frac{\mathbf{V}^i-\mathbf{V}^{i-1}}{\Delta\sigma^-}\right)\Bigg\}, \tag{20}$$

where no ambiguity is introduced by dropping the + and − superscripts on the remaining horizontal velocity gradient terms.

An alternative expression for w_{vdc} is obtained from (17) if it is assumed that the horizontal derivatives $[(\nabla\cdot\mathbf{V})^i]^+ = [(\nabla\cdot\mathbf{V})^i]^-$. Using (18a) and (18d), and recognizing that $\Delta z = H\Delta\sigma/(a-b)$, (17) reduces to

$$\begin{aligned}\frac{w_{\text{vdc}}^{i+1}}{\Delta\sigma^+} - w_{\text{vdc}}^i\left(\frac{1}{\Delta\sigma^+}+\frac{1}{\Delta\sigma^-}\right) + \frac{w_{\text{vdc}}^{i-1}}{\Delta\sigma^-} &= -\frac{1}{2}\Bigg\{\frac{H}{(a-b)}[(\nabla_\sigma\cdot\mathbf{V})^{i+1}-(\nabla_\sigma\cdot\mathbf{V})^{i-1}] \\ &\quad -\left[\frac{(\sigma^{i+1}-b)}{(a-b)}\nabla\eta+\frac{(\sigma^{i+1}-a)}{(a-b)}\nabla h\right]\cdot\left(\frac{\mathbf{V}^{i+1}-\mathbf{V}^i}{\Delta\sigma^+}\right) \\ &\quad +\left[\frac{(\sigma^{i-1}-b)}{(a-b)}\nabla\eta+\frac{(\sigma^{i-1}-a)}{(a-b)}\nabla h\right]\cdot\left(\frac{\mathbf{V}^i-\mathbf{V}^{i-1}}{\Delta\sigma^-}\right)\Bigg\}.\end{aligned} \tag{21}$$

Previous investigators (Lynch and Naimie 1993; Muccino et al. 1997) have used an expression for w_{vdc} that is equivalent to (21). However, results from Muccino et al. (1997) show that vertical velocities obtained using this discretization do not agree with analytic values. In section 5, we demonstrate that (20) yields vertical velocity estimates that are essentially identical to the analytic solution, while (21) yields estimates that are significantly inferior. As shown in appendix B, this owes to (20) being mathematically consistent with (3), while (21) is not.

b. Discretization of ADJ

Recall that the adjoint solution (9) consists of the sum of the traditional solution w_{trad} (the solution of the governing equation using the bottom boundary condition and neglecting the surface boundary condition) plus a correction. Thus, the numerical solution proceeds by first finding w_{trad} by discretizing (1):

$$\frac{w_{\text{trad}}^i - w_{\text{trad}}^{i-1}}{\Delta z^-} = -\frac{1}{2}[(\nabla\cdot\mathbf{V})^i + (\nabla\cdot\mathbf{V})^{i-1}]. \tag{22}$$

Using the chain rule, this becomes

$$\begin{aligned}\frac{w_{\text{trad}}^i - w_{\text{trad}}^{i-1}}{\Delta\sigma^-} &= -\frac{1}{2}\Bigg\{\frac{H}{a-b}[(\nabla_\sigma\cdot\mathbf{V})^i+(\nabla_\sigma\cdot\mathbf{V})^{i-1}] \\ &\quad -\left[\frac{(\sigma^i+\sigma^{i-1}-2b)}{(a-b)}\nabla\eta+\frac{(\sigma^i-\sigma^{i-1}-2a)}{(a-b)}\nabla h\right]\cdot\left[\frac{\mathbf{V}^i-\mathbf{V}^{i-1}}{\Delta\sigma^-}\right]\Bigg\}.\end{aligned} \tag{23}$$

The calculation is initiated using the bottom boundary condition, and then marched up the water column; no matrix solver is required. Once w_{trad} is known, w_c is easily computed algebraically and added to w_{trad} to yield the adjoint solution, w_{adj}.

c. Comparison of VDC and ADJ

Consider VDC first. The second-order equation should admit, in addition to the solution of the associated first-order equation, terms that are linear and constant in z. For example, suppose the vertical velocity that satisfies the first-order equation (1) is

$$w(z) = g(z). \tag{24a}$$

Consider a different vertical velocity field with addition terms, linear and constant in z:

$$w(z) = g(z) + c_1 z + c_2, \tag{24b}$$

where c_1 and c_2 are constants. The second derivatives of both (24a) and (24b) are

$$\frac{\partial w^2}{\partial z^2} = \frac{\partial g^2}{\partial z^2}. \tag{25}$$

Thus, the additional terms in (24b) are transparent in VDC. Furthermore, since the VDC solution is forced to satisfy both boundary conditions, these terms take on a form such that $w(z)$ satisfies both boundary conditions.

Now consider ADJ with $W_f/H^2 = 0$. In this case, (9) can be written in the form of (24b):

$$w_{\text{adj}}(z) = w_{\text{trad}}(z) + [w_s - w_{\text{trad}}(\eta)]\frac{z}{H} + [w_s - w_{\text{trad}}(\eta)]\frac{h}{H}, \tag{26}$$

and, therefore,

$$c_1 = \frac{[w_s - w_{\text{trad}}(\eta)]}{H}, \qquad c_2 = [w_s - w_{\text{trad}}(\eta)]\left(\frac{h}{H}\right). \tag{27}$$

Thus, VDC and ADJ with $W_f/H^2 = 0$ should theoretically yield the same vertical velocity solution. Indeed, this equivalence is found numerically when (20) is used

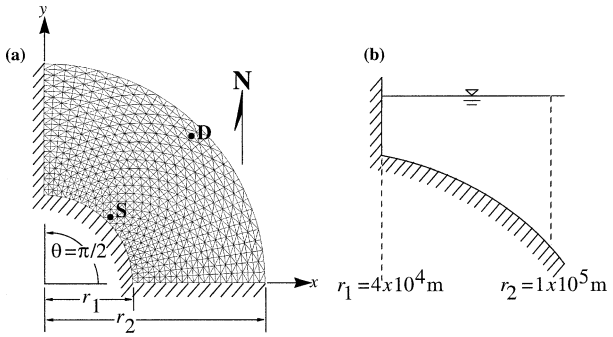

FIG. 3. The quarter-annular harbor domain with opening at $r = r_2$ and quadratic bottom: (a) plan view and (b) side view.

for the VDC solution, although it does not occur when (21) is used for the VDC solution. This is demonstrated below using two different test problems.

4. Quarter-annular harbor test case

We begin numerical tests in a quarter-annular harbor with quadratic bathymetry and periodic boundary forcing; the analytic vertical velocity for this problem is given in Muccino et al. (1997) and thus serves as a useful starting point for comparing the accuracy of these approaches. That solution is repeated in appendix A for convenience.

The geometry of the quarter-annular harbor is as in Muccino et al. (1997) and is shown in Fig. 3. The boundaries at $r = r_1 = 4 \times 10^4$ m, $\theta = 0$, and $\theta = \pi/2$ are no-flow boundaries. The open boundary, located at $r = r_2 = 1 \times 10^5$ m, is forced by an M_2 tide with frequency $\omega = 1.405 \times 10^{-4}$ s^{-1} and amplitude $\eta_0 = 0.10$ m. The bathymetry of the harbor, as shown in Fig. 3b, is quadratic in r and constant in θ, such that $h = h_0 r^2$, where $h_0 = 6.25 \times 10^{-9}$ m^{-1}.

The free-surface elevation and horizontal velocity are calculated using the analytic solution in Lynch and Officer (1985); these are calculated analytically, rather than numerically, so that any deviations of the numerical vertical velocity solution from the analytic vertical velocity solution are due entirely to the vertical velocity solution technique.

However, evaluation of horizontal velocity *derivatives* is considered to be a component of the vertical velocity calculation procedure. Thus (20), (21), and (23) are discretized in the horizontal using Galerkin finite elements with linear basis functions. The solution is evaluated using the grid shown in Fig. 3a. The grid has 825 nodes and 1536 elements in the horizontal and 32 evenly spaced sigma layers in the vertical. Results are presented here for the two representative nodes shown in the figure: node S is shallow ($h = 11.29$ m) and node D is deep ($h = 56.41$ m).

The results in Muccino et al. (1997) are for two sets of parameters and are shown at just one instant in the tidal cycle. Here, we use one set of parameters [consistent with Fig. 4 of Muccino et al. (1997): $\lambda = 6.627 + 6.627i$ and $K = 102.1$; see appendix A for the definition of these parameters] and present the vertical velocity as amplitude and phase in Fig. 4. The parameter W_f/H^2 is set to zero here; its impact on the ADJ solution is investigated next. In these figures, the analytic, ADJ, and VDC (20) amplitudes and phases are coincident, with the VDC (21) amplitude and phase differing from them. Results for different values of λ, K, and h_0 and at other nodes are not shown but are qualitatively similar, indicating that the observations regarding Fig. 4 do not depend upon particular choices of parameters or bathymetry but rather are quite general. These figures clearly show that the VDC (21) solutions have considerable error compared to the other numerical solutions. Results using higher-resolution grids (not shown) gave no indication that the VDC (21) solutions were converging to the analytic solutions, suggesting that this numerical solution is inconsistent with the original differential equation (3). A Taylor series analysis of the VDC (21) equation (appendix B) confirms this inconsistency.

Now we will consider the impact of W_f/H^2 on the ADJ solution. Recall the normalized correction profiles for various values of W_f/H^2 in Fig. 1; to obtain the actual correction, these profiles are scaled by the surface boundary condition misfit of the traditional solution (9). In the quarter-annular harbor, the magnitude of this misfit is two or three orders of magnitude smaller than w_{trad}. Thus, the ADJ correction is insignificant, regardless of the value of W_f/H^2, and ADJ essentially collapses to the traditional approach.

5. Application to the Pacific Coast of southwest Vancouver Island

The summer circulation off the western continental margin of Vancouver Island is characterized by a moderately intense upwelling of nutrients that supports high biological productivity and a lucrative commercial fishery. Circulation models (e.g., Foreman et al. 2000) have been developed to better understand both spatial and temporal variations in this upwelling, and these physical models are now being coupled to biological models in order to simulate specific components of the food chain. The accuracy of these models is highly dependent on both their adherence to mass conservation (so that nutrients are not falsely depleted or created) and the accuracy of the vertical velocities that move nutrients and biota up the water column. A circulation model for this region is thus a useful test for the vertical velocity calculations described here.

The model used here is the pseudo-nonlinear FUNDY5 (Lynch and Werner 1987) that incorporates root-mean-square tidal velocities in the bottom friction and vertical viscosity coefficients [see Foreman et al. (2000) for further details]. This model solves the three-dimensional, harmonic shallow-water equations in a sequential

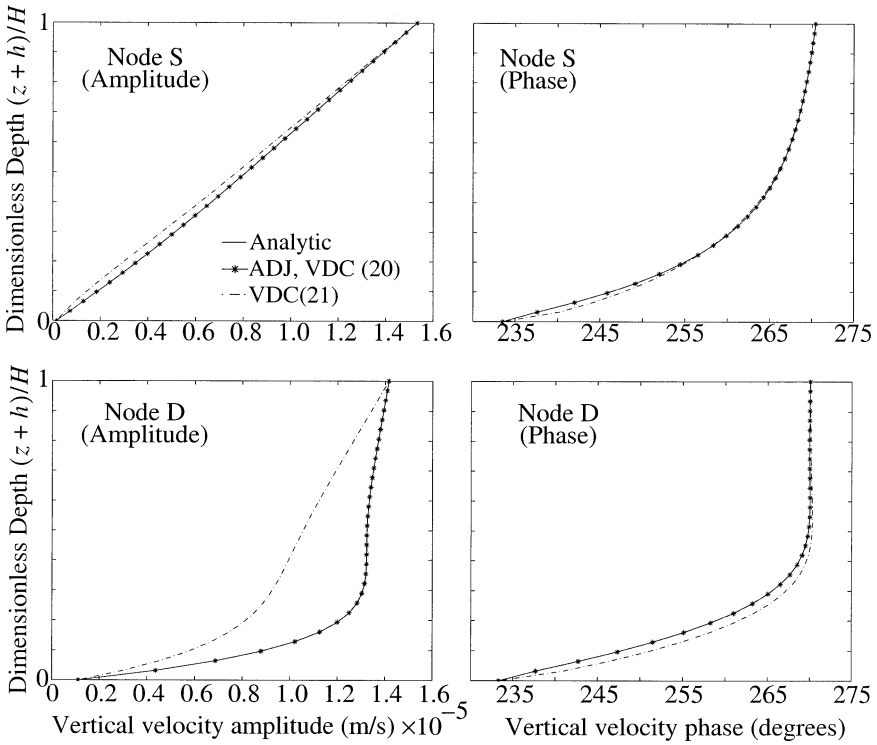

FIG. 4. Amplitudes and phases of vertical velocity in the quarter-annular harbor at node S and node D. Note that the analytic, ADJ, and VDC (20) solutions are coincident, but different from the VDC (21) solution.

manner using linear triangular finite elements. In this test application we consider only the steady-state solution resulting from steady forcing. Combined wind- and buoyancy-driven flows are forced with average winds measured at a meteorological buoy near the middle of the model domain and a three-dimensional density field that was constructed through kriging of temperature and conductivity measurements taken in late July 1998. Boundary conditions for these calculations were computed through a combination of geostrophic radiation conditions and adjustments to the surface elevations so that the vertically integrated flows passed through the boundary without any reflection. Analogous to the inversion described in Foreman et al. (2000), further boundary condition adjustments were also made to introduce a California Undercurrent consistent with observations at two current meter moorings lying along the continental slope.

The bathymetry and the horizontal discretization of the region are shown in Fig. 5. The computational grid comprises 9767 nodes horizontally and 41 evenly spaced sigma surfaces vertically. Several nodes are highlighted in the figure for future reference; each of these nodes is representative of certain regions in the domain, as detailed in Table 1. Vertical velocity profiles for nodes A–E calculated with ADJ using a range of W_f/H^2 values and VDC (21) are shown in Fig. 6. Since, the VDC (20) solution is coincident with the ADJ solution when $W_f/H^2 = 0$, it is not distinct in Fig. 6. Several observations may be made regarding these figures:

1) In all cases, the VDC (21) solution is substantially different than the ADJ solutions for any value of W_f/H^2.
2) In the deep ocean (node A), on the continental shelf (node B), and near the coast (node C), the vertical velocities are very small (order 1×10^{-5} m s^{-1}).
3) Along the sides of Barkley Canyon (nodes D and E), the vertical velocities are one to two orders of magnitude greater than at nodes A, B, and C. The ability to predict the patterns of vertical velocity in regions such as Barkley Canyon is important in understanding biological productivity (Allen et al. 2001). Of particular concern here is the fact that VDC (21) and ADJ predict opposite vertical velocity trends. On the south side of Barkley Canyon, VDC (21) predicts upwelling while ADJ predicts downwelling, and on the north side of the same canyon, VDC (21) predicts downwelling while ADJ predicts upwelling. Further insight into the vertical velocity behavior may be gained by examining the horizontal velocity field in that region at $z = -300$ m [$(z + h)/H \approx 0.4$ at nodes D and E] as illustrated in Fig. 7; this figure shows a California Undercurrent that generally follows the bathymetry toward the northwest. However, the flow cuts across the deepest parts

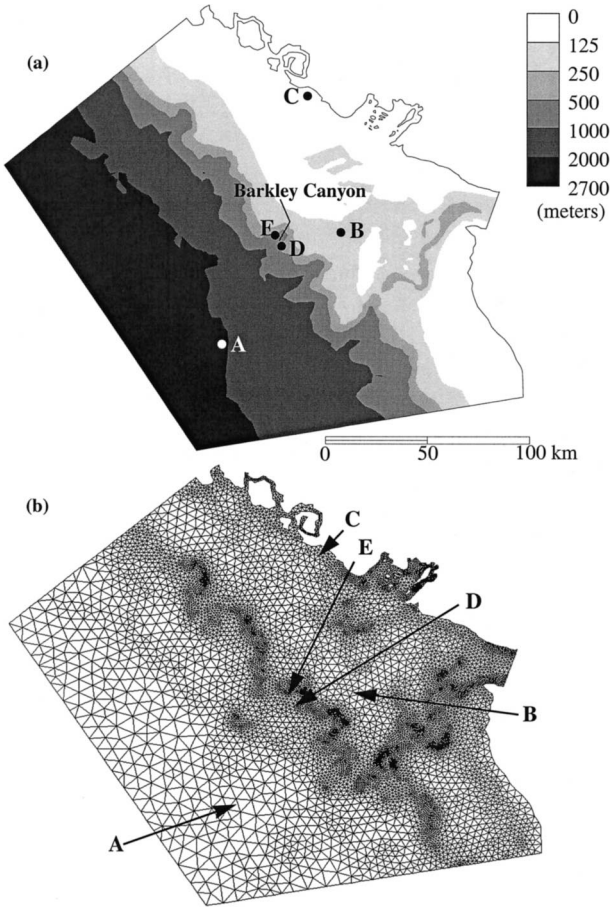

FIG. 5. The southwestern Vancouver Island domain: (a) contours of bathymetry (m) and (b) computational grid. Labeled points are discussed further in the text.

of the canyon, suggesting downwelling on the south side of the canyon and upwelling on the north side of the canyon. This is the vertical velocity behavior predicted by ADJ for all values of W_f/H^2; VDC (21) predicts the opposite.

4) Unlike results presented for the quarter-annular harbor, there is considerable dependence here of the ADJ solution on W_f/H^2 for all nodes except near the coast, at node C. This dependence indicates that the surface boundary condition misfit of the traditional solution is relatively large.

TABLE 1. Description of representative nodes in the southwestern Vancouver Island domain.

Node	Region	H (m)	Surface boundary condition misfit of traditional solution (m s^{-1})
A	Deep ocean	2020	-6.0×10^{-5}
B	Continental shelf	138	-6.7×10^{-5}
C	Coast	35	-1.5×10^{-7}
D	South Barkley Canyon	475	-1.4×10^{-3}
E	North Barkley Canyon	487	6.2×10^{-3}

5) As shown in Fig. 1, there is not much change in the vertical velocity solution obtained with values of $W_f/H^2 = 10$ and $W_f/H^2 = 100$, and thus we consider these values of W_f/H^2 to be ''large,'' in the sense that larger values will not substantially change the solution. Likewise, there is little difference in the solution obtained with values of $W_f/H^2 = 0$ and $W_f/H^2 = 0.1$, and thus we consider these values of W_f/H^2 to be ''small.''

6. Effects of local mass conservation

The previous sections have shown that the traditional, adjoint, and vertical derivative (20) solutions for vertical velocity give essentially identical results when the surface boundary condition misfit of the traditional solution is equal to zero. This misfit is readily identified as owing to errors in the horizontal solution. Integrating (1) from the bottom upward and applying the bottom boundary condition (2a) yields

$$w_{\text{trad}}(z) = -\int_{-h}^{z} \nabla \cdot \mathbf{V}\, dz - \mathbf{V}(-h) \cdot \nabla h. \quad (28)$$

Applying Liebnitz's rule to the integral in (28) yields

$$w_{\text{trad}}(z) = -\nabla \cdot \int_{-h}^{z} \mathbf{V}\, dz + \mathbf{V}(z) \cdot \nabla z. \quad (29)$$

In the interior of the water column, $\nabla z = 0$ and the vertical velocity is simply the horizontal divergence of the horizontal velocity field integrated up from the bottom. At the free surface, (29) becomes

$$w_{\text{trad}}(\eta) = -\nabla \cdot \int_{-h}^{\eta} \mathbf{V}\, dz + \mathbf{V}(\eta) \cdot \nabla \eta. \quad (30)$$

Using the surface boundary condition (2b) to replace the final term in (30) and rearranging gives

$$w_s - w_{\text{trad}}(\eta) = \frac{\partial \eta}{\partial t} + \nabla \cdot \int_{-h}^{\eta} \mathbf{V}\, dz. \quad (31)$$

The rhs of (31) is the vertically integrated continuity equation. Consequently, (31) shows that the misfit between the traditional solution evaluated at the surface and the surface boundary condition is nonzero anywhere in the domain that the horizontal velocity field does not conserve mass in the vertically integrated sense. Since numerical models solve discrete rather than continuous governing equations, discretization of the vertically integrated continuity equation in (31) must match that used to evaluate (1) and (2). Thus, local mass conservation, on the same numerical stencil used to determine w, is required if the misfit on the lhs of (31) is to be zero. If mass is not locally conserved, error is introduced into the computed vertical velocity field as it is integrated up the water column.

The quarter-annular test problem presented in section

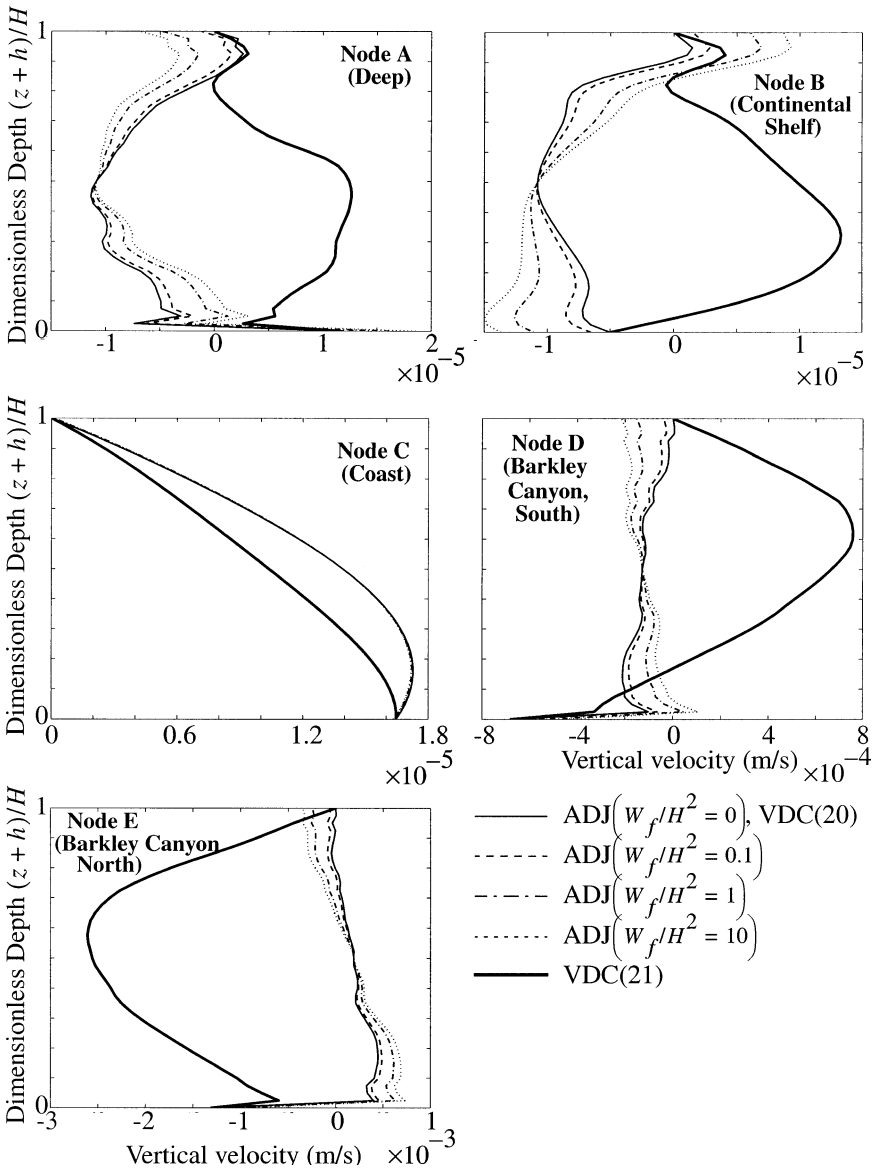

FIG. 6. Vertical velocity profiles for nodes A–E (as shown in Fig. 5) using ADJ with a range of W_f/H^2 values and VDC (20) and (21). In all cases, the VDC (20) solution is coincident with the ADJ solution for $W_f/H^2 = 0$ (see section 4c).

5 uses horizontal velocities obtained from the analytical solution, and thus these velocities satisfy the vertically integrated continuity equation exactly; the surface misfit is insignificant, and VDC (20) and ADJ with any value of the parameter W_f/H^2 give essentially identical results throughout the domain.

While finite-difference models using Arikawa C grids conserve mass on each computational cell, Galerkin finite element models are guaranteed to conserve mass only globally (Lynch 1985; Lynch and Holboke 1997) and therefore allow for nonzero local residuals in the vertically integrated continuity equation. Figure 8 illustrates the surface misfits for the Vancouver Island test problem; by (31), this plot also represents local vertically integrated continuity residuals. Considerable surface misfits are observed; regions having large misfits (and thus poor vertically integrated mass conservation) typically correspond to areas of steep bathymetric gradients. Plots of surface misfits or vertically integrated mass error such as this are easy to construct and provide a useful diagnostic tool for identifying areas where local mass conservation is relatively poor and, therefore, where significant errors are likely to exist in the vertical velocity solution.

As outlined earlier, most oceanic circulation models follow a sequential solution procedure in which the vertical velocity solution occurs separately from and with minimal feed back to the free-surface elevation and hor-

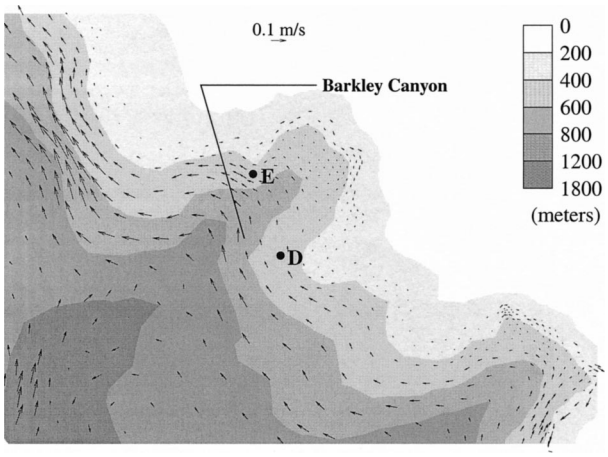

FIG. 7. Horizontal velocity field at $z = -300$ m (velocities on stretched coordinate surfaces are interpolated onto the level surface 300 m below the surface). The flow is toward the northwest, largely following the bathymetry. However, the flow cuts across the deepest part of the Barkley Canyon; this would indicate a downwelling on the south side of the canyon and an upwelling on the north side of the canyon.

izontal velocity solutions. Since mass-conservation error in the free-surface elevation and horizontal velocity solutions is the cause of the vertical velocity solution error identified above, it seems inadvisable to sacrifice the boundary condition information in favor of stricter adherence to the three-dimensional continuity equation when determining the vertical velocity. Consequently, we suggest a small value of the ADJ weighting parameter W_f/H^2 ($W_f/H^2 < 0.1$) as preferable to a high value ($W_f/H^2 > 10$).

7. Conclusions

The results presented in this paper help reconcile past uncertainty in the vertical velocity solution in three-dimensional circulation models. Specifically, we have found the following.

1) Most three-dimensional circulation models use a sequential solution procedure to solve for the free-surface elevation and velocity fields. That is, the vertically integrated continuity and the three-dimensional momentum equations are solved first for the free-surface elevation and the horizontal velocity fields; then the three-dimensional continuity equation is solved for the vertical velocity field. Solving the three-dimensional continuity equation (a first-

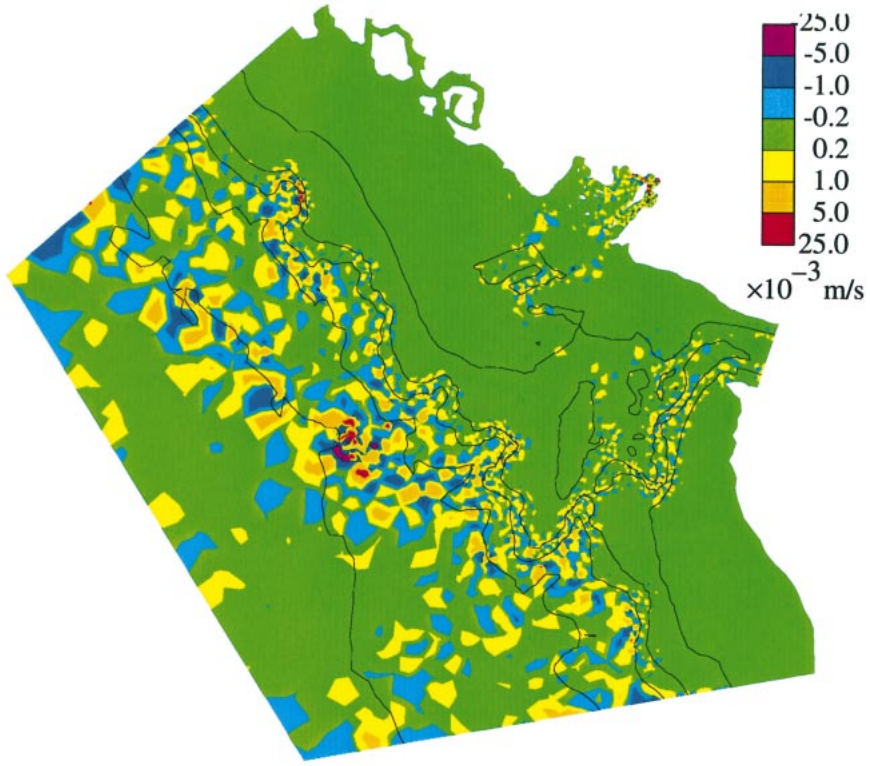

FIG. 8. Misfit between the traditional solution at the surface and the surface boundary condition for the Vancouver Island domain. Filled, colored contours represent misfits, and contour lines represent bathymetry (with the same contour intervals as Fig. 5). Residuals are largest in regions of sharply varying bathymetry.

order differential equation in the vertical coordinate) for the vertical velocity would appear to be problematic given the need to satisfy boundary conditions at both the bottom and at the free surface. However, the ''traditional'' (TRAD) vertical velocity solution, obtained by integrating the three-dimensional continuity equation upward using the bottom boundary condition, will match the surface boundary condition if the elevation and horizontal velocity fields exactly satisfy the vertically integrated continuity equation on the same numerical stencil used to determine *w*. In this case, the surface boundary condition is redundant. If the elevation and horizontal velocity fields are not locally mass conserving, the misfit between the TRAD solution and the surface boundary condition is equal to the local error in the vertically integrated continuity equation.

2) The VDC approach proposed by Lynch and Naimie (1993), in which the vertical velocity is computed from the vertical derivative of the three-dimensional continuity equation, is equivalent to an optimal, adjoint solution (ADJ) of the three-dimensional continuity equation (Muccino et al. 1997) in which the boundary conditions are preserved in lieu of stricter adherence to the continuity equation. VDC requires the solution of a tridiagonal matrix problem over the vertical while ADJ requires no matrix solution. Thus ADJ is more computationally efficient than VDC.
3) The discretization of VDC used in previous work (21) is mathematically inconsistent with the underlying differential equation (3) and, consequently, yields less accurate results than the other vertical velocity solutions we considered. This was demonstrated mathematically using Taylor series truncation error analysis and numerically in the quarter-annular harbor and Vancouver Island test cases. In the latter case, in some areas, the VDC (21) vertical velocity solutions appear to be inconsistent in both magnitude and direction with the horizontal flow field. It is important that, if VDC is used, the discretization presented in (20) be used rather than the discretization presented in (21).
4) The ADJ solution minimizes the cost functional (5), which penalizes misfits to the three-dimensional continuity equation and to the bottom and surface boundary conditions. The ADJ solution can be shown to be the sum of the TRAD solution and a linear correction. In the limit of satisfying both the bottom and free-surface boundary conditions ($W_f/H^2 = 0$) the correction is zero at the bottom and equal to the misfit of the TRAD solution and the free-surface boundary condition at the surface. In the limit of maximizing adherence to the three-dimensional continuity equation ($W_f/H^2 > 10$) the correction is a constant over the entire water column and equal to one-half of the misfit of the TRAD solution and the free-surface boundary condition.
5) If there is no misfit between the TRAD solution and the free-surface boundary condition, TRAD, ADJ, and VDC (20) give identical solutions for the vertical velocity.
6) Results from models that do not enforce strict local mass conservation, such as finite element models, will be susceptible to the vertical velocity errors described in conclusion 1. We recommend plotting maps of the error in the vertically integrated continuity equation as a diagnostic tool for determining areas in the domain that may be subject to significant vertical velocity errors. The first choice for improving the computed vertical velocity is to reduce errors in vertically integrated mass conservation, either by improved grid resolution or by smoothing the bathymetry (Oliveira et al. 2000). Mass conservation may also be improved in Generalized Wave Continuity Equation–based finite element models by increasing the primitive continuity equation weighting parameter (known as τ_0 or G) (Kolar et al. 1992, 1994). If local mass conservation cannot be achieved, we suggest use of ADJ with the weighting coefficient set to preferentially favor the surface and bottom boundary conditions ($W_f/H^2 < 0.1$).

Acknowledgments. The authors thank Chris Naimie for independently confirming that the results presented here are consistent with FUNDY5, and the two anonymous reviewers for their comments. The authors also thank Rick Thomson, Susan Allen, Dave Mackas, and the crew of the CCGS *John P. Tully* for collecting the salinity, temperature, and velocity data that were used in this study. These observations were taken during a GLOBEC Canada cruise that was cosponsored by the Natural Sciences and Engineering Research Council of Canada and the Department of Fisheries and Oceans. R. Luettich would like to acknowledge funding for this work by the Office of Naval Research award N00014-97-C-6010 and the U. S. Army Corps of Engineers Research Development Center, Coastal Inlets Research Program, award DACW 42-00-C-006. J. Muccino would like to acknowledge partial funding for this work by the National Science Foundation under OCE-9520956 and OCE-0121315.

APPENDIX A

Analytic Solution for Quarter-Annular Harbor

Consider a quarter-annular harbor with no-flow boundaries at $r = r_1$, $\theta = 0$, and $\theta = \pi/2$ and an open boundary at $r = r_2$. The open boundary is subject to periodic forcing $\eta = \mathrm{Re}\{\eta_0 e^{i\omega t}\}$. The bathymetry of the harbor is quadratic in r and constant in θ, such that $h = h_0 r^2$. The eddy viscosity, N, and bottom friction, k, vary such that

$$K = \frac{kh}{N} \quad \text{and} \quad \lambda = \sqrt{\frac{i\omega h^2}{N}} \tag{A1}$$

are constant. The analytic solutions for surface elevation and horizontal velocity (Lynch and Officer 1985) are

$$\eta(r, t) = \mathrm{Re}\{(Ar^{s_1} + Br^{s_2}) \exp(i\omega t)\}, \quad \text{(A2)}$$

$$v(r, \sigma, t) = \mathrm{Re}\{v_0(r)[1 - \delta \cosh(\lambda\sigma)]e^{i\omega t}\} \quad \text{(A3)}$$

where

$$A = \frac{\eta_0 s_2 r_1^{s_2}}{s_2 r_2^{s_1} r_1^{s_2} - s_1 r_1^{s_1} r_2^{s_2}},$$

$$B = \frac{-\eta_0 s_1 r_1^{s_1}}{s_2 r_2^{s_1} r_1^{s_2} - s_1 r_1^{s_1} r_2^{s_2}}$$

$$s_1 = -1 + \sqrt{1 - \beta^2}, \qquad s_2 = -1 - \sqrt{1 - \beta^2},$$

$$\beta^2 = (\omega^2 - i\omega\tau)/(gh_0),$$

$$\tau = \frac{N}{h^2}\left[\frac{\lambda^2 \tanh\lambda}{\lambda + \left(\frac{\lambda^2}{K} - 1\right)\tanh\lambda}\right]$$

$$v_0(r) = -\frac{g}{i\omega r}(s_1 A r^{s_1} + s_2 B r^{s_2}),$$

and g is the gravitational constant and $i = \sqrt{-1}$. The vertical velocity is (Muccino et al. 1997)

$$w(r, \sigma, t) = \mathrm{Re}\left\{2\gamma\alpha_1\delta\left[[\sigma\cosh(\lambda\sigma) + \cosh(\lambda)] - \frac{\sinh(\lambda\sigma) + \sinh(\lambda)}{\lambda}\right] + \gamma\alpha_2\left[\sigma + 1 - \frac{\delta[\sinh(\lambda\sigma) + \sinh(\lambda)]}{\lambda}\right] + 2\gamma\alpha_1[1 - \delta\cosh(\lambda)]\right\}, \quad \text{(A4)}$$

where

$$\sigma = z/h,$$

$$\gamma = \frac{gh_0}{i\omega}\exp(i\omega t),$$

$$\alpha_1 = As_1 r^{s_1} + Bs_2 r^{s_2}, \qquad \alpha_2 = As_1^2 r^{s_1} + Bs_2^2 r^{s_2},$$

$$\delta = \frac{1}{\cosh(\lambda)\left[1 + \frac{\lambda}{K}\tanh(\lambda)\right]}.$$

APPENDIX B

Consistency of VDC Eqs. (20) and (21)

Taylor series expansion yields

$$\sigma^{i+1} = \sigma^i + \Delta\sigma^+, \quad \text{(B1a)}$$

$$\sigma^{i-1} = \sigma^i - \Delta\sigma^-, \quad \text{(B1b)}$$

$$\frac{w_{\mathrm{vdc}}^{i+1}}{\Delta\sigma^+} = \frac{w_{\mathrm{vdc}}^i}{\Delta\sigma^+} + \frac{\partial w_{\mathrm{vdc}}^i}{\partial\sigma} + \frac{\Delta\sigma^+}{2}\frac{\partial^2 w_{\mathrm{vdc}}^i}{\partial\sigma^2} + \frac{(\Delta\sigma^+)^2}{6}\frac{\partial^3 w_{\mathrm{vdc}}^i}{\partial\sigma^3} + O[(\Delta\sigma^+)^3], \quad \text{(B1c)}$$

$$\frac{w_{\mathrm{vdc}}^{i-1}}{\Delta\sigma^-} = \frac{w_{\mathrm{vdc}}^i}{\Delta\sigma^-} - \frac{\partial w_{\mathrm{vdc}}^i}{\partial\sigma} + \frac{\Delta\sigma^-}{2}\frac{\partial^2 w_{\mathrm{vdc}}^i}{\partial\sigma^2} - \frac{(\Delta\sigma^-)^2}{6}\frac{\partial^3 w_{\mathrm{vdc}}^i}{\partial\sigma^3} + O[(\Delta\sigma^-)^3], \quad \text{(B1d)}$$

$$\frac{\mathbf{V}^{i+1} - \mathbf{V}^i}{\Delta\sigma^+} = \frac{\partial\mathbf{V}^i}{\partial\sigma} + \frac{\Delta\sigma^+}{2}\frac{\partial^2\mathbf{V}^i}{\partial\sigma^2} + \frac{(\Delta\sigma^+)^2}{6}\frac{\partial^3\mathbf{V}^i}{\partial\sigma^3} + O[(\Delta\sigma^+)^3], \quad \text{(B1e)}$$

$$\frac{\mathbf{V}^i - \mathbf{V}^{i-1}}{\Delta\sigma^-} = \frac{\partial\mathbf{V}^i}{\partial\sigma} - \frac{\Delta\sigma^-}{2}\frac{\partial^2\mathbf{V}^i}{\partial\sigma^2} + \frac{(\Delta\sigma^-)^2}{6}\frac{\partial^3\mathbf{V}^i}{\partial\sigma^3} + O[(\Delta\sigma^+)^3, (\Delta\sigma^-)^3], \quad \text{(B1f)}$$

$$\mathbf{V}^{i+1} - \mathbf{V}^{i-1} = (\Delta\sigma^+ + \Delta\sigma^-)\left[\frac{\partial\mathbf{V}^i}{\partial\sigma} + \frac{\Delta\sigma^+ - \Delta\sigma^-}{2}\frac{\partial^2\mathbf{V}^i}{\partial\sigma^2}\right] + O[(\Delta\sigma^+)^3, (\Delta\sigma^-)^3]. \quad \text{(B1g)}$$

Substituting appropriate Taylor series expansions into the discretized lhs of both (20) and (21) yields

$$\mathrm{lhs}_{(20),(21)} = \frac{(\Delta\sigma^+ + \Delta\sigma^-)}{2}\left\{\frac{\partial^2 w_{\mathrm{vdc}}^i}{\partial\sigma^2} + \frac{(\Delta\sigma^+ - \Delta\sigma^-)}{3}\frac{\partial^3 w_{\mathrm{vdc}}^i}{\partial\sigma^3} + O[(\Delta\sigma^+)^2, (\Delta\sigma^-)^2]\right\}. \quad \text{(B2)}$$

Explicitly retaining only the leading order term and using (14b) yields

$$\text{lhs}_{(20),(21)} = \frac{(\Delta\sigma^+ + \Delta\sigma^-)}{2}\frac{H^2}{(a-b)^2}\left\{\frac{\partial^2 w^i_{\text{vdc}}}{\partial z^2} + O[(\Delta\sigma^+ - \Delta\sigma^-), (\Delta\sigma^+)^2, (\Delta\sigma^-)^2]\right\}. \tag{B3}$$

Substituting appropriate Taylor series expansions into the discretized rhs of (20) and consolidating terms yields

$$\begin{aligned}\text{rhs}_{(20)} = -\frac{1}{2}\Bigg\{&\frac{H(\Delta\sigma^+ + \Delta\sigma^-)}{(a-b)}\left[\frac{\partial(\nabla_\sigma\cdot\mathbf{V})^i}{\partial\sigma} + \frac{(\Delta\sigma^+ - \Delta\sigma^-)}{2}\frac{\partial^2(\nabla_\sigma\cdot\mathbf{V})^i}{\partial\sigma^2}\right]\\ &-(\Delta\sigma^+ + \Delta\sigma^-)\left[\frac{(\sigma^i - b)}{(a-b)}\nabla\eta + \frac{(\sigma^i - a)}{(a-b)}\nabla h\right]\cdot\left[\frac{\partial^2\mathbf{V}^i}{\partial\sigma^2} + \frac{(\Delta\sigma^+ - \Delta\sigma^-)}{3}\frac{\partial^3\mathbf{V}^i}{\partial\sigma^3}\right]\\ &-(\Delta\sigma^+ + \Delta\sigma^-)\left[\frac{\nabla H}{(a-b)}\right]\cdot\left[\frac{\partial\mathbf{V}^i}{\partial\sigma} + \frac{(\Delta\sigma^+ - \Delta\sigma^-)}{2}\frac{\partial^2\mathbf{V}^i}{\partial\sigma^2} + \frac{[(\Delta\sigma^+)^3 + (\Delta\sigma^-)^3]}{6(\Delta\sigma^+ + \Delta\sigma^-)}\frac{\partial^3\mathbf{V}^i}{\partial\sigma^3}\right]\\ &+ O[(\Delta\sigma^+)^3, (\Delta\sigma^-)^3]\Bigg\}.\end{aligned} \tag{B4}$$

Explicitly retaining only the leading-order terms yields

$$\begin{aligned}\text{rhs}_{(20)} = -\frac{(\Delta\sigma^+ + \Delta\sigma^-)}{2}\Bigg\{&\frac{H}{(a-b)}\frac{\partial(\nabla_\sigma\cdot\mathbf{V})^i}{\partial\sigma} - \left[\frac{(\sigma^i - b)}{(a-b)}\nabla\eta + \frac{(\sigma^i - a)}{(a-b)}\nabla h\right]\cdot\frac{\partial^2\mathbf{V}^i}{\partial\sigma^2}\\ &-\left[\frac{\nabla H}{(a-b)}\right]\cdot\frac{\partial\mathbf{V}^i}{\partial\sigma} + O[(\Delta\sigma^+ - \Delta\sigma^-), (\Delta\sigma^+)^2, (\Delta\sigma^-)^2]\Bigg\}.\end{aligned} \tag{B5}$$

Using the chain rule on the second and third terms and regrouping yields

$$\begin{aligned}\text{rhs}_{(20)} = -\frac{(\Delta\sigma^+ + \Delta\sigma^-)}{2}\frac{H}{(a-b)}\Bigg(&\frac{\partial}{\partial\sigma}\left\{(\nabla_\sigma\cdot\mathbf{V})^i - \frac{(a-b)}{H}\left[\frac{(\sigma^i - b)}{(a-b)}\nabla\eta + \frac{(\sigma^i - a)}{(a-b)}\nabla h\right]\cdot\frac{\partial\mathbf{V}^i}{\partial\sigma}\right\}\\ &+ O[(\Delta\sigma^+ - \Delta\sigma^-), (\Delta\sigma^+)^2, (\Delta\sigma^-)^2]\Bigg).\end{aligned} \tag{B6}$$

Upon implementation of (14), (41) becomes

$$\text{rhs}_{(20)} = -\frac{(\Delta\sigma^+ + \Delta\sigma^-)}{2}\frac{H^2}{(a-b)^2}\left\{\frac{\partial}{\partial z}(\nabla\cdot\mathbf{V})^i + O[(\Delta\sigma^+ - \Delta\sigma^-), (\Delta\sigma^+)^2, (\Delta\sigma^-)^2]\right\}. \tag{B7}$$

Setting $\text{lhs}_{(20)}$ equal to $\text{rhs}_{(20)}$ yields

$$\frac{\partial^2 w^i_{\text{vdc}}}{\partial\sigma^2} = -\frac{\partial}{\partial z}(\nabla\cdot\mathbf{V})^i + O[(\Delta\sigma^+ - \Delta\sigma^-), (\Delta\sigma^+)^2, (\Delta\sigma^-)^2], \tag{B8}$$

which is consistent with the original differential equation (3). If $\Delta\sigma^+ = \Delta\sigma^-$, this discretization is second order in the stretched vertical coordinate, while if $\Delta\sigma^+ \neq \Delta\sigma^-$, it is first order.

Similar Taylor series substitutions on the rhs of (21) yield

$$\begin{aligned}\text{rhs}_{(21)} = -\frac{(\Delta\sigma^+ + \Delta\sigma^-)}{2}\Bigg\{&\frac{H}{(a-b)}\frac{\partial(\nabla_\sigma\cdot\mathbf{V})^i}{\partial\sigma} - \frac{1}{2}\left[\frac{(\sigma^i - b)}{(a-b)}\nabla\eta + \frac{(\sigma^i - a)}{(a-b)}\nabla h\right]\cdot\frac{\partial^2\mathbf{V}^i}{\partial\sigma^2}\\ &-\left[\frac{\nabla H}{(a-b)}\right]\cdot\frac{\partial\mathbf{V}^i}{\partial\sigma} + O[(\Delta\sigma^+ - \Delta\sigma^-), (\Delta\sigma^+)^2, (\Delta\sigma^-)^2]\Bigg\}.\end{aligned} \tag{B9}$$

Performing the same sequence of manipulations described above yields

$$\text{rhs}_{(21)} = -\frac{(\Delta\sigma^+ + \Delta\sigma^-)}{2}\frac{H^2}{(a-b)^2}\left\{\frac{\partial}{\partial z}(\nabla\cdot\mathbf{V})^i + \frac{1}{2}\left[\frac{(\sigma^i - b)}{(a-b)}\nabla\eta + \frac{(\sigma^i - a)}{(a-b)}\nabla h\right]\cdot\frac{\partial^2\mathbf{V}^i}{\partial\sigma^2} + O[(\Delta\sigma^+ - \Delta\sigma^-), (\Delta\sigma^+)^2, (\Delta\sigma^-)^2]\right\}. \quad \text{(B10)}$$

Setting $\text{lhs}_{(21)}$, (38), equal to $\text{rhs}_{(21)}$ yields

$$\frac{\partial^2 w^i_{\text{vdc}}}{\partial\sigma^2} = -\frac{\partial}{\partial z}(\nabla\cdot\mathbf{V})^i - \frac{1}{2}\left[\frac{(\sigma^i - b)}{(a-b)}\nabla\eta + \frac{(\sigma^i - a)}{(a-b)}\nabla h\right]\cdot\frac{\partial^2\mathbf{V}^i}{\partial\sigma^2} + O[(\Delta\sigma^+ - \Delta\sigma^-), (\Delta\sigma^+)^2, (\Delta\sigma^-)^2]. \quad \text{(B11)}$$

which is clearly not consistent with the original differential equation (3).

REFERENCES

Allen, S. E., C. Vindeirinho, R. E. Thomson, M. G. G. Foreman, and D. L. Mackas, 2001: Physical and biological processes over a submarine canyon during an upwelling event. *Can. J. Fish. Aquat. Sci.,* **59,** 671–684.

Blumberg, A. F., and G. L. Mellor, 1987: A description of a three-dimensional coastal ocean circulation model. *Three-dimensional Coastal Ocean Models,* C. N. K. Mooers, Ed., Coastal and Estuarine Sciences, Vol. 4, Amer. Geophys. Union, 1–16.

Foreman, M. G. G., R. E. Thomson, and C. L. Smith, 2000: Seasonal current simulations for the western continental margin of Vancouver Island. *J. Geophys. Res.,* **105** (C8), 19 665–19 698.

Haidvogel, D. B., and A. Beckmann, 1999: Three-dimensional ocean models. *Numerical Ocean Circulation Modeling,* Imperial College Press, 121–162.

Kolar, R. L., W. G. Gray, and J. J. Westerink, 1992: An analysis of the mass conserving properties of the generalized wave continuity equation. *Computational Methods in Water Resources IX,* Vol. 2, T. Russell et al., Eds., Computational Mechanics Publications, 537–544.

——, ——, ——, and R. A. Luettich Jr., 1994: Shallow water modeling in spherical coordinates: Equation formulation, numerical implementation and application. *J. Hydraul. Res.,* **32,** 3–24.

Lynch, D. R., 1985: Mass balance in shallow water simulations. *Commun. Appl. Numer. Methods,* **1,** 153–159.

——, and C. B. Officer, 1985: Analytic test cases for three-dimensional hydrodynamic models. *Int. J. Numer. Methods Fluids,* **5,** 529–543.

——, and F. E. Werner, 1987: Three-dimensional hydrodynamics on finite elements. Part II: Linearized harmonic model. *Int. J. Numer. Methods Fluids,* **7,** 871–909.

——, and ——, 1991: Three-dimensional hydrodynamics on finite elements. Part I: Nonlinear time-stepping model. *Int. J. Numer. Methods Fluids,* **12,** 507–533.

——, and C. E. Naimie, 1993: The M2 tide and its residual on the outer banks of the Gulf of Maine. *J. Phys. Oceanogr.,* **23,** 2222–2253.

——, and M. J. Holboke, 1997: Normal flow boundary conditions in 3D circulation models. *Int. J. Numer. Methods Fluids,* **25,** 1185–1205.

Muccino, J. C., and A. F. Bennett, 2002: Generalized inversion of the Korteweg–de Vries equation. *Dyn. Atmos. Oceans,* **35,** 227–263.

——, W. G. Gray, and M. G. G. Foreman, 1997: Calculation of vertical velocity in three-dimensional, shallow water equation, finite element models. *Int. J. Numer. Methods Fluids,* **25,** 779–802.

Oliveira, A., A. B. Fortunato, and A. M. Baptista, 2000: Mass balance in Eulerian–Lagrangian transport simulations in estuaries. *J. Hydraul. Eng.,* **126,** 605–614.